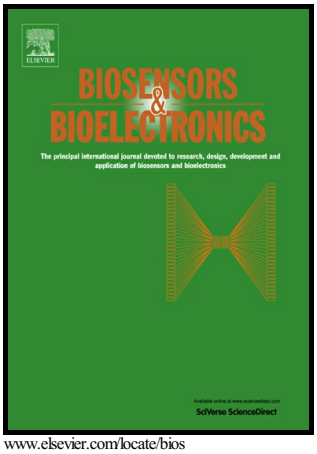

www.elsevier.com/locate/bios

Perovskite-type calcium titanate nanoparticles as novel matrix for designing sensitive electrochemical biosensing

Lei Wang, Juan Li, Mengjie Feng, Lingfeng Min, Juan Yang, Suhua Yu, Yongcai Zhang, Xiaoya Hu, Zhanjun Yang

PII: S0956-5663(17)30314-7
DOI: http://dx.doi.org/10.1016/j.bios.2017.05.004
Reference: BIOS9716

To appear in: *Biosensors and Bioelectronic*

Received date: 8 February 2017
Revised date: 28 April 2017
Accepted date: 3 May 2017

Cite this article as: Lei Wang, Juan Li, Mengjie Feng, Lingfeng Min, Juan Yang, Suhua Yu, Yongcai Zhang, Xiaoya Hu and Zhanjun Yang, Perovskite-type calcium titanate nanoparticles as novel matrix for designing sensitiv electrochemical biosensing, *Biosensors and Bioelectronic* http://dx.doi.org/10.1016/j.bios.2017.05.004

Perovskite-type calcium titanate nanoparticles as novel matrix for designing sensitive electrochemical biosensing

Lei Wang,[1] Juan Li,[1,*] Mengjie Feng,[1] Lingfeng Min,[2] Juan Yang,[1] Suhua Yu,[1] Yongcai Zhang,[1] Xiaoya Hu,[1] Zhanjun Yang[1,]**

[1]*School of Chemistry and Chemical Engineering, Yangzhou University, Yangzhou 225002, PR China*

[2]*Clinical Medical School of Yangzhou University, Subei People's Hospital of Jiangsu Province, Yangzhou, Jiangsu 225001, PR China*

Abstract: In this work, novel perovskite-type calcium titanate nanoparticles ($CaTiO_3$NPs) were for the first time exploited for the immobilization of proteins and the development of electrochemical biosensor. The $CaTiO_3$NPs were synthesized with a simple and cost-effective route at low temperature, and characterized by scanning electron microscopy, X-ray photoelectron spectroscopic spectrum, electrochemical impedance spectrum, UV-visible spectroscopy, Fourier transform infrared spectrum, and cyclic voltammetry, respectively. The results indicated that $CaTiO_3$NPs exhibited large surface area, and greatly promoted the direct electron transfer between enzyme molecules and electrode surface. The immobilized enzymes on this matrix retained its native bioactivity and exhibited a surface controlled, quasi-reversible two-proton and two-electron transfer reaction with an electron transfer rate of 3.35 s^{-1}. Using glucose oxidase as model, the prepared glucose biosensor showed a high sensitivity of 14.10 ± 0.5 mA M^{-1} cm^{-2}, a wide linear range of 7.0×10^{-6} to 1.49×10^{-3} M, and a low detection limit of 2.3×10^{-6} M at signal-to-noise of 3. Moreover, the biosensor also possessed good reproducibility, excellent selectivity and acceptable storage life. This research provided a new-type and promising perovskite nanomaterials for the development of efficient biosensors.

Keywords: Perovskite nanomaterials, $CaTiO_3$ nanoparticles; Biosensor; Enzymes; Direct electrochemistry

* Corresponding author. Tel./Fax: +86-514-87975244.

E-mail address: lijuan@yzu.edu.cn (J. Li); zjyang@yzu.edu.cn (Z.J. Yang)

1. Introduction

In recent years, perovskite structured materials and their derivatives have been widely studied in fundamental research and high potential for technical applications because of their different physical properties (Dawber et al., 2005; Kan et al., 2005; Maksimov et al., 2007; Moreira et al., 2009). Their electronic structure and photophysical properties are gaining more and more attention of many researchers. Particularly, great efforts have been devoted to the synthesis and study of titanate materials such as $ATiO_3$ (A=Ca, Sr, Ba, Pb) (Orhan et al., 2005; Lima et al., 2006; De Lazaro et al., 2007; Longo et al., 2008). $CaTiO_3$ is an important semiconductor with a band gap energy of 3.2 eV (Lozano-Sánchez et al., 2016). Due to its attractive catalytic, dielectric and photoelectric properties, $CaTiO_3$ has been exploited as catalysts, semiconductor, electrodes, dielectric material, luminescent material, solar cells and so on (Wang et al., 2007; Cavalcante et al., 2008; Marques et al., 2008; Moreira et al., 2009; Yang et al., 2008; Lozano-Sánchez et al., 2015). Recently, perovskite structured materials have begun to attract increasing interest in biosensing fields because of their special properties. Hu et al. reported very early the synthesis of nanoplated bismuth titanate sub-mcirospheres and their derivatives, one type of inorganic perovskite materials, for immobilization of protein and electrochemical biosensing applications (Chen et al., 2009; Hu et al., 2011). However, since then very few researches on the fabrication of biosensors based on perovskite materials have been reported to date (Cai et al., 2014). To the best of our knowledge, perovskite structured $CaTiO_3$NPs have not been reported for biosensing applications so far.

Since the first glucose biosensor developed by Clark and Lyons in 1962, electrochemical biosensor has been widely applied in many areas because of rapid and sensitive detection as well as simple and convenient operations (Wang, 2006; Hahn et

al., 2012). In particular, electrochemical biosensor has been of high interest in rapid measurement of glucose concentration in serum samples due to great significance for the diagnosis and treatment of diabetes (Mizutani and Yabuki, 1997; Yu et al., 2003; Dai et al., 2009). Glucose oxidase (GOx) has been extensively used to monitor the blood glucose level in diabetics for its high biochemical stability and catalytic ability to glucose (Vamvakai et al., 2006; Xu et al., 2010). However, the realization of the direct electron transfer on bare electrode is extremely difficult because the active center (flavin-adenine dinucleotide, FAD) of GOx is deeply embedded in a protective protein shell (Meng et al., 2009). During the past decades, various nanostructured materials, such as metal, carbon, semiconductor, and magnetic nanomaterials have been utilized to develop novel electrochemical glucose biosensors due to their high surface-volume ratio and unique physical properties (Liu and Ju, 2003; Yang et al., 2015; Wu et al., 2007a; Nadzhafova et al., 2007; Kang et al., 2009; Qiu et al., 2009; Xiao et al., 2010; Ammam and Fransaer, 2012; Palanisamy et al., 2014b). It has been proved that the direct electron transfer between the active center of enzymes and electrode could be achieved easily by the immobilization of GOx on nanomaterials modified electrodes (Deng et al., 2009; Wu et al., 2009). Although various kinds of nanomaterials have been exploited for electrochemical glucose biosensing applications, the exploration of novel and low-cost matrix for the development of high-performance electrochemical glucose biosensor is still highly desirable.

Herein, perovskite structured $CaTiO_3$NPs were synthesized with a simple and low-temperature route from low-melting-point of $Ca(NO_3)_2{\cdot}4H_2O$ and high-reactive-activity TiO_2. Then $CaTiO_3$ perovskite NPs were for the first time employed as a novel matrix for the immobilization of enzyme and electrochemical biosensing. The resultant $CaTiO_3$ perovskite NPs and enzyme biosensor were

characterized using scanning electron microscopy, electrochemical impedance spectra, UV-visible spectroscopy, Fourier transform infrared spectra, and cyclic voltammetry. This perovskite nanomaterial has large surface area and provides a biocompatible environment to enhance direct electron transfer between enzyme and electrode surface. A pair of well-defined and sensitive redox peaks of enzyme could be obtained at $CaTiO_3$NPs modified electrode. Using GOx as a model, a novel electrochemical glucose biosensor was constructed for rapid detection of glucose. The proposed glucose biosensor showed excellent performances such as high sensitivity, low detection limit, and good selectivity, which could be successfully applied to detect glucose in human serum samples at the applied potential of -0.45 V.

2. Materials and methods

2.1 Materials and Reagents

The glucose oxidase (EC 1.1.3.4, 108 U mg^{-1}, from Aspergillus niger) was supplied by Amresco (http://www.amresco-inc.com). D-(+)-Glucose and chitosan were purchased from Sigma-Aldrich (http://www.sigma-aldrich.com). $Ca(NO_3)_2{\cdot}4H_2O$ and P25 TiO_2 powders were purchased from Shanghai SuYi Chemical Reagent Co., Ltd. A stock solution of D-glucose was prepared and allowed to mutarotate at room temperature for 24 h before measurements. Phosphate buffer solution (PBS) was the mixture of 0.1 M Na_2HPO_4 and NaH_2PO_4, and its pH was adjusted with H_3PO_4 or NaOH solution. All other chemicals and reagents were of analytical grade, and prepared using the distilled water.

2.2 Apparatus

Electrochemical measurements were carried out on a CHI 852C electrochemical workstation (Co., CHI, Shanghai Chenhua, China). All experiments were carried out

with a three-electrode system. The modified glassy carbon electrode (GCE) was as the working electrode, a platinum wire and a saturated calomel electrode (SCE) were used as the auxiliary electrode and the reference electrode, respectively. The cyclic voltammetric experiments were carried out at a scan rate of 100 mV s^{-1} in an electrochemical cell filled with 10.0 mL of PBS. All pH measurements were made with S-25 digital pH-meter with glass combination electrode. Scanning electron micrographs (SEM) were obtained with a Hitachi S-4800 scanning electron microscope (Japan) at an acceleration voltage of 15 kV. X-ray photoelectron spectroscopic (XPS) spectrum analysis was measured with an ESCALAB 250Xi spectrometer (USA). Electrochemical impedance spectroscopy (EIS) measurements were performed on an Autolab/PGSTAT30 (Metrohm, Netherlands) in 0.1 M KCl solution containing 5 mM $K_3[Fe(CN)_6]/K_4[Fe(CN)_6]$. Its amplitude of the applied sine wave potential was 5 mV. The impedance spectra were recorded at a bias potential of 190 mV within the frequency range from 0.05 to 10 KHz. Fourier transform infrared (FT-IR) spectra were measured with a Tensor 27 spectrometer (Bruker Co., Germany). UV-vis spectra were recorded using UV-2550 spectrophotometer (Shimadzu Co., Japan).

2.3 The preparation of perovskite-type $CaTiO_3$ nanoparticles

Perovskite-type $CaTiO_3$NPs were simply synthesized using our previous method (Li et al., 2011). Briefly, the powders of 1.18 g $Ca(NO_3)_2{\cdot}4H_2O$ and 0.4 g P25 TiO_2 nanocrystals were weighed into a corundum crucible. The crucible was heated in a Muffle furnace from room temperature to 600 °C, and kept at 600 ^oC for 10 h. Then the crucible was allowed to cool to ambient temperature naturally. Next, the residue

white fluffy powders were directly collected for characterization and biosensing experiments.

2.4 The preparation of electrochemical enzyme biosensor

The GCE was firstly treated with 0.3 and 0.05 μm alumina slurry (Buhler), and rinsed alternately with distilled water and ethanol three times. Then the cleaned GCE was dried with high purity nitrogen stream. Next, 3.0 mg of $CaTiO_3$NPs were dispersed in 1.0 mL of 0.5% chitosan solution with ultrasonication, and then 10 mg of GOx was added into 1.0 mL of $CaTiO_3$-chitosan suspension, and kept stirring at a slow speed for 15 minutes. Afterwards, 5.0 μL of the ultimate suspension was dropped on the surface of the pretreated GCE, and dried at 4 °C in refrigerator to obtain firm film. The prepared GOx/$CaTiO_3$NPs-chitosan/GCE was stored at 4 °C in refrigerator before the use.

3. Results and discussion

3.1 Characterizations of the synthesized $CaTiO_3$NPs, and glucose biosensor

Due to the excellent capability of film formation, nontoxicity, biocompatibility, mechanical strength, and good water permeability (Kang et al., 2009), chitosan solution here was used to disperse $CaTiO_3$NPs to form a stable $CaTiO_3$NPs-chitosan film for the immobilization of GOx. The presence of chitosan also provides a good microenvironment for the immobilized GOx molecules. The morphology of the synthesized perovskite-type $CaTiO_3$NPs were investigated by scanning electron microscopy. Fig. A(a) showed the SEM image of the synthesized $CaTiO_3$ perovskite NPs, and uniform nanosized particles could be observed with an average diameter of 30-80 nm. Fig. A(b) exhibited the SEM image of the $CaTiO_3$NPs-chitosan composite film. It could be seen that the $CaTiO_3$NPs were distributed homogeneously into chitosan film, which provided an efficient and potential platform for the

immobilization of enzyme molecules and fabrication of biosensors. When GOx molecules were trapped into the $CaTiO_3$NPs-chitosan composite, different surface morphology was presented in Fig. A(c). The SEM image of GOx/$CaTiO_3$NPs-chitosan showed the bigger island-like protein structure, which indicated that the GOx has been uniformly immobilized on $CaTiO_3$NPs surface. X-ray photoelectron spectroscopic (XPS) spectrum analysis was also used for the quantitative measurement of $CaTiO_3$NPs, $CaTiO_3$NPs-chitosan, and GOx/$CaTiO_3$NPs-chitosan (shown in Fig. S1, Supporting Information). The XPS spectrum of $CaTiO_3$NPs showed characteristic Ca2p peak at 346.7 eV, Ti2p peak at 458.4 eV, and O1s peak at 530.2 eV. As seen from the XPS spectrum of $CaTiO_3$NPs-chitosan, a clear N1s peak at 400.2 eV was observed except characteristic Ca2P, Ti2p, and O1s peaks of $CaTiO_3$NPs, indicating the formation of $CaTiO_3$NPs-chitosan composite. The XPS spectra of GOx/$CaTiO_3$NPs-chitosan showed a strong N1s peak at 400.3 eV with same characteristic Ca2P, Ti2p, and O1s peaks, which is also much stronger than that of $CaTiO_3$NPs-chitosan, suggesting the presence of GOx molecules in $CaTiO_3$NPs-chitosan composite.

Preferred position for Fig. 1

Electrochemical impedance spectroscopy is a powerful tool to characterize the surface properties of the electrode and the electron transport process. The impedance spectrum is presented as Nyquist plot including a semicircle part and a liner part. The semicircle at the high frequency corresponds to the electron-transfer in the limiting process, whose diameter represents the electron transfer resistance (R_{ct}), and the straight line at the low frequency corresponds to the dispersion process. The Nyquist plots of different modified electrodes in the frequency range of 0.05 Hz to 10 KHz were displayed in Fig. 1B. The R*ct* value of the pretreated GCE was about 15 Ω

(curve a) (Yang et al., 2009), while the chitosan/GCE showed the bigger R*ct* value of about 82 Ω (curve b), suggesting that the chitosan film has formed on the surface of GCE. In the case of the $CaTiO_3$NPs-chitosan modified GCE, its R*ct* further increased to 156 Ω (curve c). After GOx molecules were loaded in $CaTiO_3$NPs-chitosan, GOx/$CaTiO_3$NPs-chitosan/GCE displayed the biggest R*ct* value of 308 Ω. This result indicated that GOx has been successfully immobilized into the composite film.

The UV-vis spectrum was used to investigate the native conformation and bioactivity of GOx immobilized on $CaTiO_3$ perovskite NPs. The UV-vis spectra of $CaTiO_3$NPs, native GOx and GOx/$CaTiO_3$NPs-chitosan were presented in Fig. 1C. There were no obvious absorption peaks for the $CaTiO_3$ perovskite NPs in the range of 240-550 nm. But as for the native GOx molecules, the absorption band at 273 nm was attributed to the characteristic peak of polypeptide chains in protein structure, and other two weak peaks at 380 nm and 454 nm were assigned to the characteristic of the oxidized form of flavin group in protein structure (Shan et al., 2010). The GOx immobilized on $CaTiO_3$ perovskite NPs also showed three characteristic peaks, and their position and shape of the absorption peaks were in agreement with those of the native GOx, indicating that the immobilized GOx on $CaTiO_3$NPs film maintained its native structure.

FT-IR spectroscopy was also used to characterize that the state of GOx loaded in the $CaTiO_3$ perovskite NPs structure. The FT-IR spectra of the $CaTiO_3$NPs, $CaTiO_3$NPs-chitosan, native GOx, and GOx/$CaTiO_3$NPs-chitosan were shown in Fig. 1D. $CaTiO_3$NPs showed no obvious absorption peaks, while $CaTiO_3$NPs-chitosan displayed the characteristic peaks of chitosan. In term of the native GOx, there were two characteristic peaks at 1649 and 1561 cm^{-1}, which were corresponded to the amide I and amid II bands of the enzymes, respectively. When GOx was immobilized

into $CaTiO_3$NPs-chitosan, two characteristic adsorption bands at 1630 and 1568 cm^{-1} with a slight shift were also observed from the FT-IR spectrum of GOx/$CaTiO_3$NPs-chitosan. This result indicated that enzyme molecules were successfully captured in $CaTiO_3$NPs-chitosan composite film.

3.2 The electrochemical behavior of GOx/$CaTiO_3$NPs-chitosan/GCE

Fig. 2 showed the cyclic voltammograms of different modified GCEs in 0.1 M N_2-saturated PBS at a scan rate of 100 mV s^{-1}. It could be seen that there was no redox peaks for chitosan/GCE (curve a) and $CaTiO_3$NPs-chitosan/GCE (curve b). The GOx/chitosan/GCE showed a typical pair of redox peaks (curve c). While in comparison with GOx/chitosan/GCE (curve c), GOx/$CaTiO_3$NPs-chitosan/GCE exhibited a pair of more distinct and better-defined redox peaks at -0.412 V and -0.459 V (curve d), indicating that $CaTiO_3$NPs greatly promote the direct electron transfer between the enzyme and the electrode. What's more, the reduction peak current of GOx/$CaTiO_3$NPs-chitosan/GCE was about 2.3 times as large as that of GOx/chitosan/GCE. In addition, the peak potential separation was 47 mV, which is much smaller than that of 80 mV obtained at GOx/graphene-chitosan/GCE was (Kang et al., 2009), indicating the faster electron transfer between the redox-active site of GOx (the cofactor FAD) and GCE surface (Deng et al., 2009).

Preferred position for Fig. 2

The effect of the scan rate on the cyclic voltammetric behavior at GOx/$CaTiO_3$NPs-chitosan/GCE was shown in Fig. 3A. It could be clearly seen that anodic and cathodic peak currents (I_{pa} and I_{pc}) of GOx/$CaTiO_3$NPs-chitosan/GCE increased linearly with the increase of the scan rate from 10 to 300 mV s^{-1}. The linear regression equations were I_{pa}=0.0688+0.00429V, R^2=0.9947 and I_{pc}=-0.14183-0.00489V, R^2=0.9808 (inset a of Fig. 3A). In addition, the ratio of I_{pa} to

I_{pc} was approximately equal to 1, indicating a quasi-reversible surface-controlled process. The logarithm plot of cathodic peak current versus logarithm of the scan rate showed a linear relationship (inset b of Fig. 3A). The linear regression equation was $\log I_{pc}$= -1.77+0.747log$v$ (R^2=0.9808), and the slope value was close to the theoretical slope for thin layer electrochemical behavior (Bard and Faulkner, 2001). According to the formula Γ*=Q/nFA (where Γ* is the surface coverage, Q is the charge consumed in the reaction, n is the number of electrons transferred, F is the Farady constant, and A is the electrode area), the Γ* of GOx on surface of the modified electrode was calculated to be 1.62×10^{-11} mol cm^{-2} from the integration of the reduction peak of the GOx/$CaTiO_3$NPs-chitosan/GCE at 100 mV s^{-1}. This value was larger than that of 7.82×10^{-12} mol cm^{-2}, 2.86×10^{-12} mol cm^{-2} and 9.8×10^{-12} mol cm^{-2} obtained at GOx/Au-dihexadecyl phosphate (Wu et al., 2007b), GOx/bare GCE (Zhang et al., 2007) and GOx/Au nanoparticles/carbon paste electrode (Liu and Ju, 2003), respectively. In addition, the charge-transfer coefficient and the apparent electron transfer rate constant for the proposed enzyme electrode were calculated to be 0.5 and 3.35 s^{-1}. The ks value was larger than those of 1.56, 1.7, 1.96, 2.83 and 3.12 s^{-1} reported previously (Guiseppi-Elie et al., 2002; Deng et al., 2008; Kang et al., 2009; Hui et al., 2013; Yang et al., 2015), indicating that $CaTiO_3$NPs promoted the fast electron transfer between redox-active site of enzyme and the surface of electrode.

The solution pH effect also can influence the cyclic voltammetric response of GOx/$CaTiO_3$ NPs-chitosan/GCE and was tested in the pH range from 5.0 to 9.0. As shown in Fig. 3B, the anodic and cathodic peak potentials shifted negatively with increasing pH values, and the peak currents also changed obviously. Apparently, the current response reached the maximum at pH 7.0, indicating that pH 7.0 was an optimal value for direct electron transfer of GOx on $CaTiO_3$ NPs-chitosan/GCE (inset

a of Fig. 3B). Moreover, the plot of the formal potential vs. pH produced a slope of -46.4 mV pH^{-1} (inset b of Fig. 3B), which was close to the theoretical value of -58.6 mV pH^{-1} (Deng et al., 2009), suggesting the two-electron and two-proton involving in the electron transfer process.

Preferred position for Fig. 3

3.3 The mechanism of the quantitative detection of glucose

To testify the feasibility of electrochemical biosensing of glucose, the cyclic voltammograms of $CaTiO_3$NPs-chitosan/GCE and GOx/$CaTiO_3$NPs-chitosan/GCE in nitrogen- and air-saturated pH 7.0 PBS with or without glucose were investigated in Fig. 4. Although the reduction current increased at a more negative potential than -0.4 V, no peaks were observed at $CaTiO_3$NPs-chitosan/GCE in nitrogen- and air-saturated PBS (shown in Fig. 4A). Conversely, GOx/$CaTiO_3$NPs-chitosan/GCE showed a pair of redox peaks in both N_2-saturated and air-saturated PBS solution (Fig. 4B). Moreover, a great increase in reduction peak current and an obvious decrease in oxidation peak current could be observed from the cyclic voltammogram of GOx/$CaTiO_3$NPs-chitosan/GCE in air-saturated PBS (Fig. 4B). These results proved that GOx/$CaTiO_3$NPs-chitosan/GCE has an obvious electrocatalytic process toward the reduction of dissolved oxygen. In the presence of oxygen, regenerated GOx (FAD) leaded to the increase of the reduction peak current of FAD. The phenomenon could be interpreted according to equations 1 and 2 (Liu and Ju, 2003).

$$GOx(FAD) + 2e^- + 2H^+ \leftrightarrow GOD(FADH_2) \quad [1]$$

$$GOx(FADH_2) + O_2 \rightarrow GOD(FAD) + H_2O_2 \quad [2]$$

$$Glucose + GOx(FAD) \rightarrow GOx(FADH_2) + Gluconolactone \quad [3]$$

When glucose was added to the air-saturated PBS, the reduction current of GOx/$CaTiO_3$NPs-chitosan/GCE decreased gradually with the increase of glucose

concentration. This was caused by an enzyme-catalyzed reaction as showed in equation 3. The glucose restrained the electrocatalytic reaction, which thus reduced concentration of GOx (FAD). However, the reduction current of $CaTiO_3$NPs-chitosan/GCE showed no obvious changes after addition of different concentration of glucose in air-saturated PBS. Based on the decease mentioned above, a glucose biosensor was thus developed in this work.

Preferred position for Fig. 4

3.4 Performance of the proposed glucose biosensor

Fig. 5A showed a typical current-time plot at GOx/$CaTiO_3$NPs-chitosan/GCE on successive injection of glucose in 10 mL pH 7.0 air-saturated stirring PBS (the optimal potential for the amperometric detection of glucose was chosen as -0.45 V). The electrochemical biosensor reached 95 % of the steady-state current within less than 8 s. This also indicated that the perovskite-type $CaTiO_3$NPs could be used as a novel matrix for the construction of biosensors. The calibration curve (inset of Fig. 5A) of the proposed glucose biosensor showed a linear range from 7.0×10^{-6} M to 1.49×10^{-3} M with a correlation coefficient of 0.9995 and a high sensitivity of 14.10 ± 0.5 mA M^{-1} cm^{-2}. In addition, the detection limit was calculated to be 2.3 μM (S/N=3). Table 1 showed the comparison of analytical performance between the present biosensor and other types of enzyme electrodes. It is obvious that the present biosensor possessed much better performances such as sensitivity and detection limit.

Preferred position for Fig. 5

Preferred position for Table 1

3.5 Interference study and detection of glucose in human serum samples.

The interference test was performed by adding 0.2 mM glucose, 0.1 mM uric acid (UA) and 0.1 mM ascorbic acid (AA) in 0.1 mM pH 7.0 PBS with stirring. As shown

in Fig. 5B, a clear current response appeared upon the addition of 0.2 mM glucose to pH 7.0 PBS. However, there was no apparent amperometric response by addition of 0.1 mM AA and UA to the system. But injecting 0.2 mM glucose into the solution again, a clear current response was also observed. Moreover, the current response was almost close to the value obtained in absence of the interferents. These results demonstrated that the proposed biosensor possessed high selectivity for glucose in the presence of those endogenously coexisted electroactive substances.

To demonstrate the practical application of the glucose biosensor, the glucose level in human serum from a local hospital was analyzed. The serum glucose concentration was measured to be 4.3 mM by the proposed biosensor, which was close to value of 4.12 mM measured by enzyme catalytic spectrophotometry method. Then, 0.1 mM and 0.2 mM glucose were added to the serum samples, and the recoveries were 104.8 % and 103.8 % with the relative standard deviations of 3.15 % and 1.78 %, respectively. The results indicated the proposed glucose biosensor could be used in the detection of real serum samples.

3.6 Reproducibility and stability of the glucose biosensor

In order to measure the repeatability of the biosensor, five enzyme electrodes prepared independently were used to detect the same concentration of glucose. The relative standard deviation was calculated to be 2.1% at a glucose concentration of 1.0 mM, indicating that the biosensor has acceptable reproducibility. When not in use, GOx/$CaTiO_3$NPs-chitosan/GCE was stored in 0.1 M pH 7.0 PBS at 4 ^{o}C. Within 3 weeks no obvious decrease in amperometric response to glucose was observed. Its current response still retained 93% of its initial response after 25 days. These results demonstrated that perovskite structured $CaTiO_3$NPs can provide a good microenvironment to retain the bioactivity of enzyme molecules immobilized on

them.

4. Conclusion

In this study, perovskite-type $CaTiO_3$NPs were simply synthesized, and then dispersed in chitosan solution to immobilize enzyme molecules. Based on the direct electron transfer of GOx on modified electrode, a novel and sensitive electrochemical glucose biosensor was developed for the first time. $CaTiO_3$ perovskite NPs as a new type of support matrix were characterized with various techniques, which provided a favorable environment to enhance direct electron transfer between enzyme and electrode surface, and to maintain the excellent biological activity of loaded enzyme molecules. The GOx immobilized into $CaTiO_3$NPs-chitosan composite exhibited a surface-controlled, quasi-reversible two-electron and two-proton transfer process with a large electron transfer rate constant. The $CaTiO_3$NPs-based electrochemical glucose biosensor showed low detection limit, wide linear range and acceptable reproducibility and stability, and also can be applied to the determination of glucose in serum. This work exploited potential and efficient perovskite nanomaterials for the immobilization of proteins and biosensing applications.

Acknowledgments

This work was financially supported by National Natural Science Foundation of China (21475116, 21575125 and 81302016), Qinglan Project of Jiangsu Province, Priority Academic Program Development of Jiangsu Higher Education Institution (PAPD), High-end talent support program of Yangzhou University, the National Natural Science Foundation of Jiangsu Province (BK20130455, BK20140101), and Six Talent Peaks Project of Jiangsu Province for Juan Li and Lingfeng Min (WSN-106). In addition, much thanks to The Testing Center of Yangzhou University due to all the characterizations.

Reference

Ammam, M., Fransaer, J., 2012. Biotechnol. Bioeng. 109, 1601-1609.

Bard, A.J., Faulkner, L.R., Electrochemical Methods: Fundamentals and Applications, second ed., Wiley, New York, 2001.

Cai, B., Zhao, M.G., Wang, Y., Zhou, Y., Cai, H., Ye, Z.Z., Huang, J.Y., 2014. Ceram. Int. 40, 8111-8116.

Cai, C., Chen, J., 2004. Anal. Biochem. 332, 75-83.

Cavalcante, L.S., Marques, V.S., Sczancoski, J.C., Escote, M.T., Joya, M.R., Varela, J.A., Santos, M.R.M.C., Pizani, P.S., Longo, E., 2008. Chem. Eng. J. 143, 299-307.

Ceh, M., Gu, H., Mullejans, H., Recnik, A., 1997. J. Mater. Res. 12, 2438-2446.

Chen, X.H., Hu, J.Q., Chen, Z.W., Feng, X.M., Li, A.Q., 2009. Biosens. Bioelectron. 24, 3448-3454.

Dai, Z.H., Shao, G.J., Hong, J.M., Bao, J.C., Shen, J., 2009. Biosens. Bioelectron. 24, 1286-1291.

Dawber, M., Rabe, K.M., Scott, J.F., 2005. Rev. Mod. Phys. 77, 1083-1130.

De Lazaro, S., Milanez, J., De Figueiredo, A.T., Longo, V.M., Mastelaro, V.R., De Vicente, F.S., 2007, Appl. Phys. Lett. 90, 091906.

Deng, C.Y., Chen, J.H., Chen, X.L., Xiao, C.H., Nie, L.H., Yao, S.Z., 2008. Biosens. Bioelectron. 23, 1272-1277.

Deng, S.Y., Jian, G.Q., Lei, J.P., Hu, Z., Ju, H.X., 2009. Biosens. Bioelectron. 25, 373-377.

Guiseppi-Elie, A., Lei, C., Baughman, R.H., 2002. Nanotechnology 13, 559–564.

Hahn, Y.B., Ahmad, R., Tripathy, N., 2012. Chem. Commun. 48, 10369-10385.

Hu, J.Q., Yu, Y., Guo, H., Chen, Z.W., Li, A.Q., Feng, X.M., Li, B.M., Hu, G.Q., 2011.

J. Mater. Chem. 21, 5352-5359.

Hui, J.N., Cui, J.W., Xu, G.Q., Adeloju, S.B., Wu, Y.C., 2013. Mater. Lett. 108, 88-91.

Inoue, M., Rodriguez, A.P., Takagi, T., Katase, N., Kubota, M., Nagai, N., Nagatsuka, H., Nagaoka, N., Takagi, S., Suzuki, K.J., 2010, Biomater. Appl. 24, 657-672.

Jang, H.D., Kim, S.K., Chang, H., Roh, K.M., Choi, J.W., Huang, J.X., Biosens. Bioelectron. 2012. 38, 184-188.

Kan, D.S., Terashima, T., Kanda, R., Masuno, A., Tanaka, K., Chu, S.C., 2005. Nat. Mater. 4, 816-819.

Kang, X.H., Wang, J., Wu, H., Aksay, I.A., Liu, J., Lin, Y.H., 2009. Biosens. Bioelectron. 25, 901-905.

Lee, M.C., Kabilan, S., Hussain, A., Yang, X.P., Blyth, J., Lowe, C., 2004. Anal. Chem. 76, 5748-5755.

Li, J., Zhang, Y.C., Wang, T.X., Zhang, M., 2011. Mater. Lett. 65, 1556-1558.

Lima, R.C., Espinosa, J.W.M., Gurgel, M.F.C., Paris, E.C., Leite, E.R., Joya, R., 2006. J. Appl. Phys. 100, 034917.

Liu, S.Q., Ju, H.X., 2003. Biosens. Bioelectron. 19, 177-183.

Liu, S.Q., Sun, Y.M., 2007. Biosens. Bioelectron. 22, 905-911.

Liu, Y., Wang, M.K., Zhao, F., Xu, Z.A., Dong, S.J., 2005. Biosens. Bioelectron. 21, 984-988.

Longo, V.M., De Figueiredo, A.T., De Lazaro, S., Gurgel, M.F., Costa, M.G.S., Paiva-Santos, C.O., 2008. J. Appl. Phys. 104, 023515.

Lozano-Sánchez, L.M., Méndez-Medrano, M.G., Colbeau-Justin, C., Rodríguez-López, J.L., Hernández-Uresti, D.B., Obregón, S., 2016. Chem. Commun. 84, 36-39

Lozano-Sánchez, L.M., Obregón, S., Díaz-Torres, L.A., Lee, S.W., Rodríguez-

González, V., 2015. J. Mol. Catal. A Chem. 410, 19-25.

Maksimov, E.G., Matsko, N.L., Ebert, S.V., Magnitskaya, M.V., 2007. Ferroelectrics 354, 19-38.

Mani, V., Devadas, B., Chen, S.M., 2013. Biosens. Bioelectron. 4, 309-315.

Marques, V.S., Cavalcante, L.S., Sczancoski, J.C., Volanti, D.P., Espinosa, J.W.M., Joya, M.R., Santos, M.R.M.C., Pizani, P.S., Varela, J.A., Longo, E., 2008. Solid State Sci. 10, 1056-1061

Meng, L., Jin, J., Yang, G.X., Lu, T.H., Zhang, H., Cai, C.X., 2009. Anal. Chem. 81, 7271-7280.

Miao, Z.L., Wang, P.Y., Zhong, A.M., Yang, M.F., Xu, Q., Hao, S.R., Hu, X.Y., 2015. J. Electroanal. Chem. 756, 153-160.

Mizutani, F., Yabuki, S., 1997. Biosens. Bioelectron. 12, 1013-1020.

Moreira, M.L., Paris, E.C., do Nascimento, G.S., Longo, V.M., Sambrano, J.R., Mastelaro, V.R., Bernadi, M.I.B., Andres, J., Varela, J.A., Longo, E., 2009. Acta Mater. 57, 5174-5185.

Nadzhafova, O., Etienne, M., Walcarius, A., 2007. Electrochem. Commun. 9, 1189-1195.

Orhan, E., Varela, J.A., Zenatti, A., Gurgel, M.F.C., Pontes, F.M., Leite, E.R., 2005. Phys. Rev. B 71, 085113.

Palanisamy, S., Karuppiah, C., Chen, S.M., 2014a. Colloid Surface B 114, 164-169.

Palanisamy, S., Karuppiah, C., Chen, S.M., Periakaruppan, P., 2014b. Electroanalysis 26, 1984-1993.

Qiu, J.D., Peng, H.P., Liang, R.P., Xia, X.H., 2009. Biosens. Bioelectron. 25, 1447-1453.

Shan, D., Zhang, J., Xue, H.G., Ding, S.N., Cosnier, S., 2010. Biosens. Bioelectron.

25, 1427-1433.

Tang, S., Wang, X.Z., Lei, J.P., Hu, Z., Deng, S.Y., Ju, H.X., 2010. Biosens. Bioelectron. 26, 432-436.

Unnikrishnan, B., Palanisamy, S., Chen, S.M., 2013. Biosens. Bioelectron. 39, 70-75.

Vamvakai, V., Tsagaraki, K., Chaniotakis, N., 2006. Anal. Chem. 78, 5538-5542.

Wang, D.A., Guo, Z.G., Chen, Y.M., Hao, J.M., Liu, W.M., 2007. Inorg. Chem. 46, 7707-7709.

Wang, J., 2006. Biosens. Bioelectron. 21, 1887-1892.

Wang, Y.L., Liu, L., Li, M.G., Xu, S.D., Gao, F., 2011. Biosens. Bioelectron. 30, 107-111.

Wu, H., Wang, J., Kang, X.H., Wang, C.M., Wang, D.H., Liu, J., Aksay, A.I., Lin, Y.H., 2009. Talanta 80, 403-406.

Wu, S., Ju, H.X., Liu, Y., 2007a. Adv. Funct. Mater. 17, 585-592.

Wu, Y.H., Hu, S.S., 2007b. Bioelectrochemistry 70, 335-341.

Xiao, C.H., Chu, X.C., Wu, B.H., Pang, H.L., Zhang, X.H., Chen, J.H., 2010. Talanta 80, 1719-1724.

Xu, X., Jiang, S.J., Hu, Z., Liu, S.Q., 2010. ACS Nano 4, 4292-4298.

Yang, G.J., Huang, J.L., Meng, W.J., Shen, M., Jiao, X.A., 2009. Anal. Chim. Acta. 647, 159-166.

Yang, X.F., Fu, J.X., Jin, C.J., Chen, J.A., Liang, C.L., Wu, M.M., Zhou, W.Z. 2010. J. Am. Chem. Soc. 132, 14279-14287.

Yang, X.F., Williams, I.D., Chen, J., Wang, J., Xu, H.F., Konishi, H.M., Pan, Y.X., Liang, C.L., Wu, M.M., 2008. J. Mater. Chem. 18, 3543-3546.

Yang, Z.J., Cao, Y., Li, J., Jian, Z.Q., Zhang, Y.C., Hu, X.Y., 2015. Anal. Chim. Acta. 871, 35-42.

Yang, Z.J., Huang, X.C., Zhang, Y.C., Li, J., Xu, Q., Hu, X.Y., 2012. Electrochim. Acta 70, 325-330.

Yu, J.H., Liu, S.Q., Ju, H.X., 2003. Biosens. Bioelectron. 19, 401-409.

Zhang, J.D., Feng, M.L., Tachikawa, H., 2007. Biosens. Bioelectron. 2, 3036-3041.

Figure captions

Fig. 1. (A) SEM images of the perovskite-type $CaTiO_3$NPs (a), $CaTiO_3$NPs-chitosan film (b) and GOx/$CaTiO_3$NPs-chitosan (c); (B) Nyquist polts of EIS for bare (a), chitosan (b), $CaTiO_3$NPs-chitosan (c) and GOx/$CaTiO_3$NPs-chitosan (d) modified GCEs; (C) UV-vis absorption spectra of $CaTiO_3$NPs, GOx and GOD/$CaTiO_3$NPs-chitosan; (D) FT-IR spectra of $CaTiO_3$NPs, $CaTiO_3$NPs-chitosan, GOx and GOx/$CaTiO_3$NPs-chitosan.

Fig. 2. Cyclic voltammograms for(a-d) chitosan/GCE, $CaTiO_3$/chitosan/GCE, GOD/chitosan/GCE and GOD/$CaTiO_3$/chitosan/GCE in N_2-saturated 0.1 M pH 7.0 PBS at a scan rate of 100 mV s^{-1}.

Fig. 3. (A) cyclic voltammograms of the GOx/$CaTiO_3$NPs-chitosan /GCE in 0.1 M pH 7.0 N_2-saturated PBS at 10, 20, 50, 80, 100, 150, 200 and 300 mV s^{-1} (from inside to outside), inset a: plots of anodic and cathodic peak currents vs. scan rate, inset b: plot of logarithm of i_{pc} vs. logarithm of v; and (B) Cyclic voltammograms of the GOx/$CaTiO_3$NPs-chitosan/GCE in N_2-saturated 0.1 M PBS with different pH values of (a-e) 5.0, 6.0, 7.0, 8.0 and 9.0 at a scan rate of 100 mV s^{-1}, inset a: plot of peak currents vs. pH, and inset b: plot of formal potentials vs. pH.

Fig. 4. (A) Cyclic voltammograms of the $CaTiO_3$NPs-chitosan/GCE in 0.1 M pH 7.0 N_2-saturated PBS, air-saturated PBS, and air-saturated PBS including 0.5 and 1.0 mM glucose at a scan rate of 100 mV s^{-1}, and (B) cyclic voltammograms of the GOx/$CaTiO_3$NPs-chitosan/GCE in 0.1 M pH 7.0 N_2-saturated PBS and air-saturated PBS including 0, 0.5, 1.0, 1.5, 2.0, and 3.0 mM glucose.

Fig. 5. (A) Typical current-time plot of the GOx/$CaTiO_3$NPs-chitosan/GCE on successive addition of glucose into air-saturated 0.1 M pH 7.0 PBS at the applied potential of -0.45V, inset: calibration curve of the GOx/$CaTiO_3$NPs-chitosan/GCE for glucose, and (B) Amperometric response of the GOx/$CaTiO_3$NPs-chitosan/GCE to 0.2 mM glucose, 0.1 mM AA and 0.1 mM UA in pH 7.0 PBS at -0.45V applied potential.

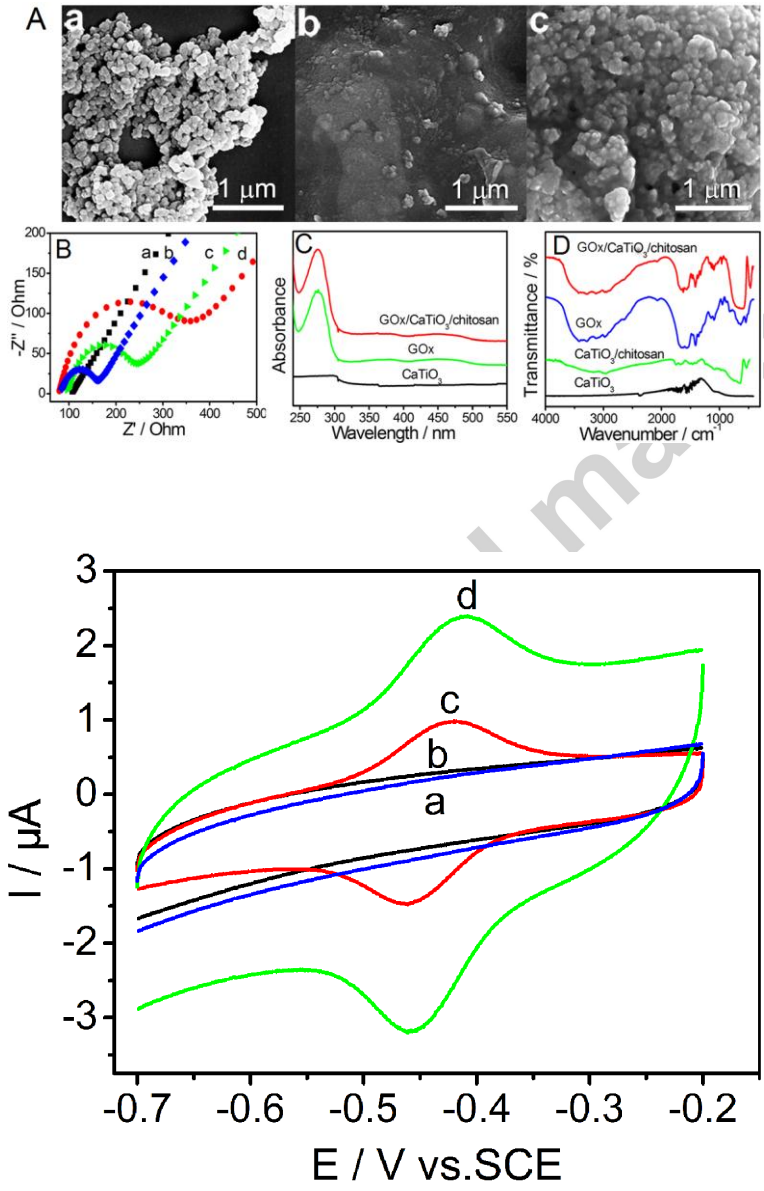

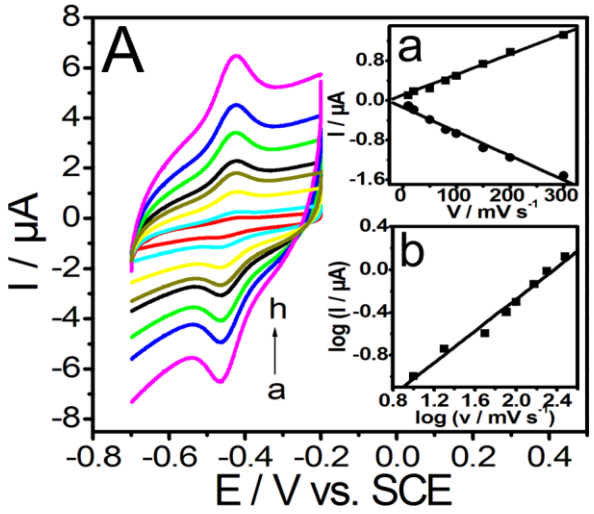
A
a
h
a
I / μA
V / mV s-1
log (I / μA)
log (v / mV s-1)
E / V vs. SCE

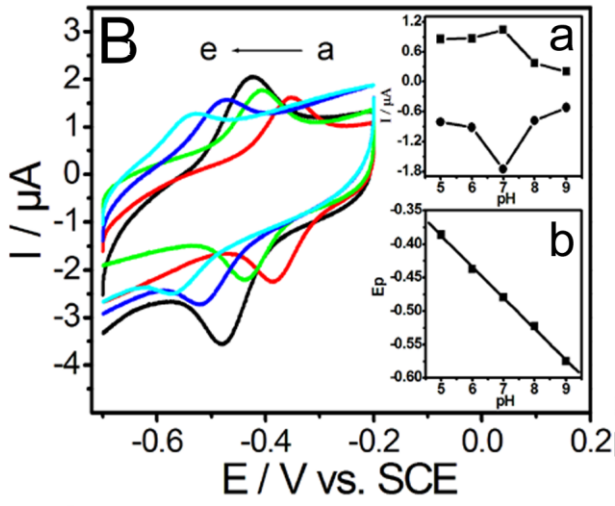
B
e
a
a
b
I / μA
pH
Ep
E / V vs. SCE

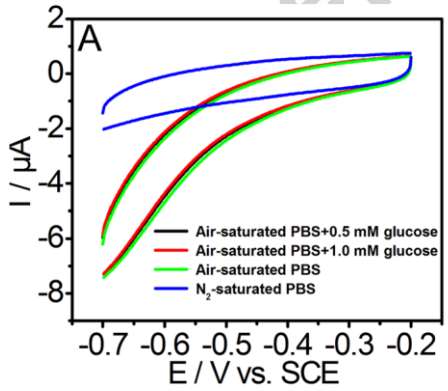
A
Air-saturated PBS+0.5 mM glucose
Air-saturated PBS+1.0 mM glucose
Air-saturated PBS
N2-saturated PBS
I / μA
E / V vs. SCE

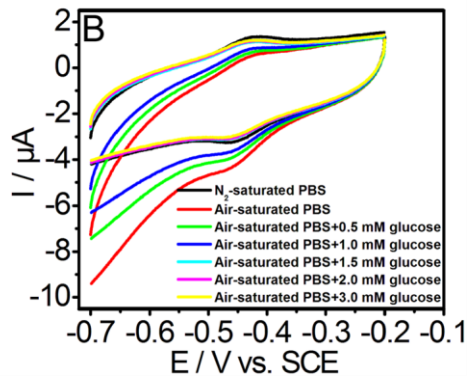
B
N2-saturated PBS
Air-saturated PBS
Air-saturated PBS+0.5 mM glucose
Air-saturated PBS+1.0 mM glucose
Air-saturated PBS+1.5 mM glucose
Air-saturated PBS+2.0 mM glucose
Air-saturated PBS+3.0 mM glucose
I / μA
E / V vs. SCE

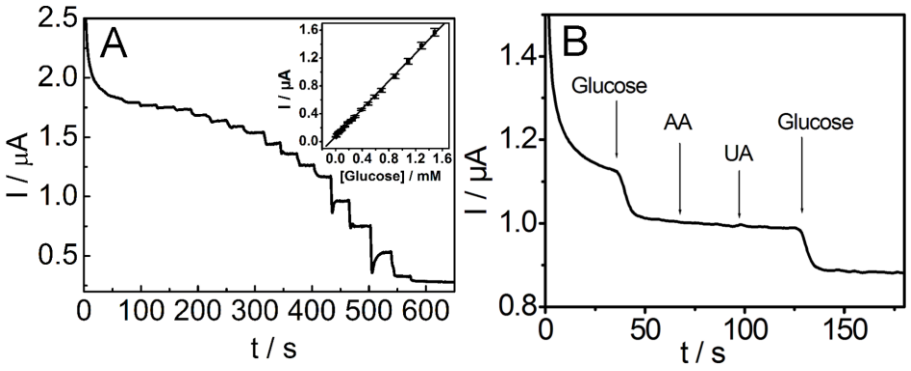

Table 1 Comparison of analytical performance between GOD/$CaTiO_3$/chitosan/GCE and other modified electrodes

Electrode	Applied potential (V)	Sensitivity ($mA\ M^{-1}\ cm^{-2}$)	Detection limit (mM)	Linear range (mM)	Reference
GOD/$CaTiO_3$/chitosan/GCE	–0.45	14.10	0.0023	0.007–1.49	This work
RGO/GOx/GCE	–0.44	1.85	–	0.1–27	Unnikrishnan et al., 2013
RGO/Ag/GOx/GCE	–0.49	3.84	0.16	0.5–12.5	Palanisamy et al., 2014a
GOx/SnS_2-Nafion/GCE	–0.45	7.6	0.01	0.025–1.1	Yang et al., 2011
GOx/Pt/FCNA/GCE	–0.08	6.0	0.3	0.5–8.0	Tang et al., 2010
ERGO-MWCNT/GOx/GCE	+0.35	7.95	0.0047	0.01–6.5	Mani et al., 2013
GOx/TiO_2-graphene/GCE	–0.60	6.2	–	0.0–8.0	Jang et al., 2012
GOx/TPSP-ZnO/Nafion/GCE	–0.50	–	0.01	0.05–8.2	Dai et al., 2009
Nafion/GOx/Ag-Pdop@CNT/GCE	–0. 50	3.1	0.017	0.05–1.1	Wang et al., 2011
Silica hybrid sol-gel/GOx/GCE	+1.0	10.8	0.019	0.06–4.4	Liu and Sun, 2007
Laponite/GOx/GCE	–0.45	4.8	0.01	0.02–1.9	Shan et al., 2010

RGO: reduced graphene oxide

FCNA: flower-like carbon nanosheet aggregation

ERGO: electrochemically reduced graphene oxide.

MWCNT: multiwalled carbon nanotubes.

TPSP: tetragonal pyramid-shaped porous.

Pdop: polydopamine.

Highlights

- Perovskite-type $CaTiO_3$NPs was exploited as efficient matrix to immobilize proteins.
- A novel and sensitive electrochemical biosensor was constructed based on $CaTiO_3$NPs.

- The proposed glucose biosensor presented high sensitivity and low detection limit.
- The $CaTiO_3$NPs provided the promising perovskite nanomaterials for biosensing applications.